JOURNAL OF GEOPHYSICAL RESEARCH, VOL. 102, NO. D1, PAGES 1399–1410, JANUARY 20, 1997

Millimeter wave spectroscopic measurements over the South Pole 3. The behavior of stratospheric nitric acid through polar fall, winter, and spring

R. L. de Zafra,[1] V. Chan,[2] S. Crewell, C. Trimble,[3] and J. M. Reeves[4]

Department of Physics, State University of New York, Stony Brook

Abstract. We present data from a 9-month series of ground-based measurements of stratospheric nitric acid, made over the South Pole from mid-April 1993 to mid-January 1994. Observations were typically made at 3- to 6-day intervals. Both profiles and column densities have been retrieved from pressure-broadened millimeter-wave emission spectra. These measurements provide the first quasi-continuous series of vertical mixing ratio profiles for this species in the heart of the south polar votex. Conversion of NO_x to nitric acid by heterogeneous reactions, and its incorporation into polar stratospheric cloud (PSC) particles, along with subsequent gravitational settling, is considered to be the main denitrifying mechanism in the Antarctic stratosphere, setting up conditions for ozone destruction at the end of winter. In our observations, a small increase in HNO_3 was seen between April and the end of May, after which a rapid loss took place below 25 km. Column density above ~15 km decreased to $\leq 1/4$ its maximum within 30 days, and depletion continued until middle to late July, by which time the nitric acid column above 15 km had diminished by more than a factor of 10. The initial depletion was coincident with the onset of a rapid increase in lidar backscatter from polar stratospheric cloud formation at the same altitude range. Gas-phase depletion was tracked as a function of altitude and temperature and found to be consistent with the temperature and partial pressure relationship for formation of ternary mixtures of HNO_3, H_2SO_4, and H_2O. Depletion occurred ~3 weeks earlier in 1993 than was seen in 1992 column density measurements by *Van Allen et al.* [1995]. In late June a new layer of HNO_3 was generated in the vicinity of 40-km altitude and, subsequently, appeared to be carried downward with general vertical transport of air within the vortex. In spring, as temperatures increased, no rapid increase of gas-phase HNO_3 was seen, indicating that gravitational settling had carried PSC-accreted nitric acid to low altitudes. By the end of observations in January 1994, mixing ratios and column densities above ~15 km had not yet reached more than about half the values seen the previous April, indicating that a rather large increase in stratospheric HNO_3 occurs in the early austral fall over the south polar region.

1. Introduction

The formation of nitric acid by heterogeneous chemistry, condensation from the gas phase into aerosols at sufficiently low temperatures, and subsequent gravitational settling, is a principal means of removing NO_x from the Antarctic polar stratosphere during winter months, setting up the conditions for massive ozone destruction in the Antarctic spring. The generally warmer average temperatures and short duration of polar stratospheric cloud (PSC) events in the Arctic stratosphere limit the removal of HNO_3 and have thus far prevented the severe denoxification needed for the formation of a major "ozone hole" in the north. This very different behavior of HNO_3 in the two polar winter regions means that each must be studied separately to define the local climatology for nitric acid, and conclusions derived from one pole are not, in general, applicable to the other. We review here the information available to date, and then discuss new results from a 9-month series of millimeter-wave spectroscopic observations we have made at the heart of the Antarctic polar vortex.

[1] Also at Institute for Terrestrial and Planetary Atmospheres, State University of New York, Stony Brook.

[2] Now at Department of Mathematics, Iowa Sate University, Ames.

[3] Now at Sacramento, California.

[4] Now at Atmospheric, Oceanic, and Space Science Department, University of Michigan, Ann Arbor.

Paper number 95JD03679.
0148-0227/97/95JD-03679$09.00

The pioneering Limb Infrared Monitor of the Stratosphere (LIMS) measurements of HNO_3 in the north polar region made during the single winter of 1978-1979 revealed unexpected and puzzling behavior at high latitudes, including the apparent generation of gas-phase HNO_3 in the middle to upper stratosphere during the polar winter [e.g., *Austin et al.*, 1986; *Jackman et al.*, 1987]. Until recently only total column measurements were available for limited periods in the antarctic [*Williams et al.*, 1982; *Murcray et al.*, 1987, 1989; *Coffey et al.*, 1989; *Toon et al.*, 1989; *Van Allen et al.*, 1995], and no profile measurements were available until the launching of the Upper Atmosphere Research Satellite (UARS) in September 1991. In particular, direct information was lacking on the degree of removal as a function of altitude, the details of the removal process, and the subsequent fate of HNO_3 condensed onto stratospheric aerosols. Although the appearance of nitric acid in the winter upper stratosphere had been noted, neither its evolution with time nor the measurement of high-latitude stratospheric profiles over any significant portion of an annual cycle were available.

Recently, data from the Cryogenic Limb Array Etalon Spectrometer (CLAES) [*Roche et al.*, 1993, 1994; *Kawa et al.*, 1995] and the Microwave Limb Sounder (MLS) [*Santee et al.*, 1995] instruments on board UARS have begun to clarify some of the issues listed above. In this paper, we add to this information by showing mixing ratio profiles derived from data gathered every few days during the 9-month period from mid-April 1993 to mid-January 1994 by a ground-based millimeter-wave spectrometer located at the South Pole.

2. Experimental Method and Data Reduction

Spectra were recorded by using a high sensitivity cryogenically cooled heterodyne receiver in conjunction with a 512 channel filterbank spectrometer. The heterodyne receiver is sensitive in both its sidebands with equal gain (±5%). The filterbank has a resolution of 1 MHz/channel, which is enough to define pressure-broadened line shapes up to an altitude of about 50 km, while the total spectral span of 512 MHz sets a low-altitude limit of about 15-16 km. HNO_3 has a complex millimeter-wave spectrum with a large number of relatively weak emission lines which individually are hard to detect. We observe a complex of lines near a band edge which are relatively strong, although these are as close as 30 MHz to one another, and thus strongly blended by pressure broadening in the lower stratosphere. A number of these emission lines are present in the two receiver sidebands, although many are quite weak (refer to Figure 2). The observed spectral output, as illustrated, is the frequency-folded combination of the two sidebands.

Spectra were taken at intervals varying from 3 to 7 days, starting on April 15, 1993, and ending on January 10, 1994. We have retrieved vertical distribution profiles from the pressure-broadened spectra by deconvolution against locally measured pressure and temperature profiles. The latter were available up to 25-30 km from balloon sondes launched at the South Pole, supplemented by daily National Meteorological Center (NMC) temperature and pressure profiles above the balloon limits. Individual line frequencies were obtained from *Crownover et al.* [1988], line strengths from F. De Lucia (private communication, 1988), and pressure broadening coefficients from *Goyette et al.* [1988].

The retrieval of vertical profiles from the pressure-blended multiple line spectra was carried out with an iterative matrix inversion method employing a vertical smoothing constraint [*Twomey*, 1977]. This method recovers profiles over the vertical range from ~15 to 48 km with good results. Additional discussion and examples are given in the appendix.

3. Results and Discussion

Figure 1 shows an overview of our results in the form of a mixing ratio contour plot derived from the 63 one-day HNO_3 profiles retrieved over the entire period of observations. We shall divide the discussion of these data into three sections, the first dealing mainly with the condensation process when gas-phase HNO_3 was rapidly withdrawn from the lower stratosphere, the second covering the midwinter phase, and the third covering the recovery phase through the spring and summer period as far as our observations extend, with some comments about the remaining unobserved period of the late summer.

3.1 Late Fall and Early Winter: The Condensation Process

The evolution of the vertical distribution of HNO_3 in the polar stratosphere during the fall to early winter period is shown in Figures 2 and 3, by means of a representative sample of emission spectra and retrieved profiles. There appears to be a small increase in the peak mixing ratio between the start of our observations in mid-April and late May (evident in Figure 1 and in the total column of nitric acid (Figure 8) but not in the sample of data shown in Figure 2). This may mark the final stages of a more pronounced increase which must have taken place earlier in the fall, to judge by behavior in the following summer (see below). The most prominent feature of the late fall-early winter period is the very rapid gas-phase depletion first seen in the data for May 28 (day 148), which continued over the next few weeks (see Figures 1 and 8). Loss continued at a much-diminished rate until at least late July. Virtually all depletion through this period appeared to occur below ~28 km, with the earliest and strongest loss occurring between 15 and 25 km (see below). Coincident with the onset of rapid loss, the University of Rome lidar at the South Pole began detecting the first significant polar stratospheric cloud backscatter, as shown in Fig-

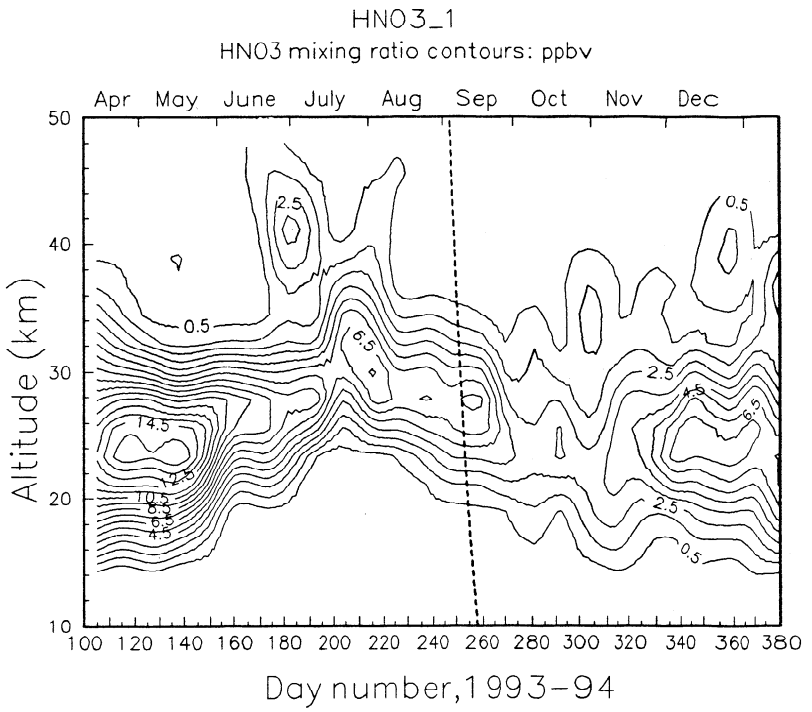

Figure 1. Contour plot from retrieved mixing ratio profiles of HNO_3 over the South Pole from April 1993 to January 1994. The interval between contours is 1 ppbv. The slanted dashed line marks the time of polar sunrise as a function of altitude. For dates of sunset and sunrise at other representative altitudes and latitudes, see Table 1. Note comments in the text for the period from about day 200 to 240.

ure 4 (G. Fiocco, personal communication, 1995). Lidar backscatter rapidly increased through the altitude range where HNO_3 loss was observed to occur, clearly demonstrating the temporal and spatial relationship of PSC growth and HNO_3 depletion, once a critical temperature range is reached. This is discussed in more detail later in this section.

Figure 5a presents a detailed contour map of HNO_3 mixing ratios versus altitude and time for the condensation period, with an overlay of local temperature profile readings taken every 2-3 days. Temperature contours at 194 and 196 K have been emphasized. Deciphering the

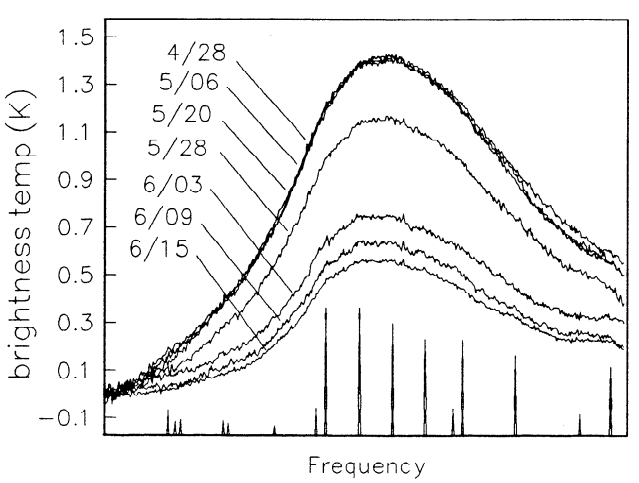

Figure 2. Representative pressure-broadened emission spectra from April 28 to June 15, 1993. The individual line positions and relative intensities are indicated at the bottom of the plot. The frequency span is 512 MHz. The three strongest lines are at 269172, 269205 and 269237 MHz.

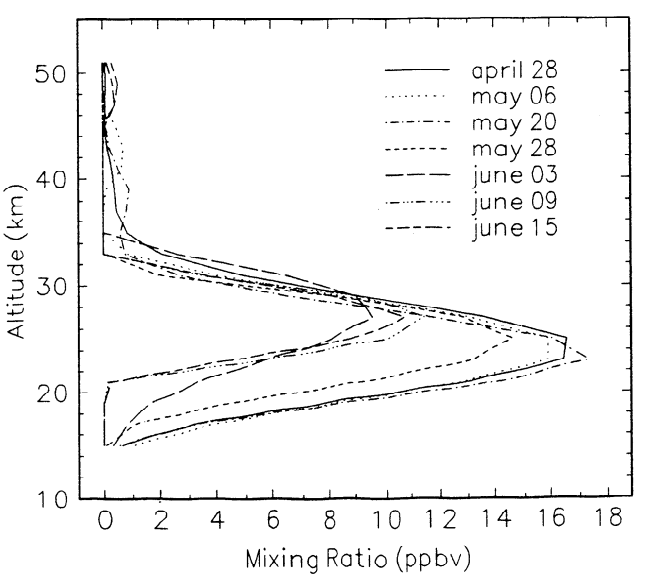

Figure 3. Profiles retrieved by deconvolution of pressure-broadened spectra of Figure 2. The small mixing ratio values above ~35 km are indicative of retrieval inaccuracies, and do not necessarily represent real HNO_3 content.

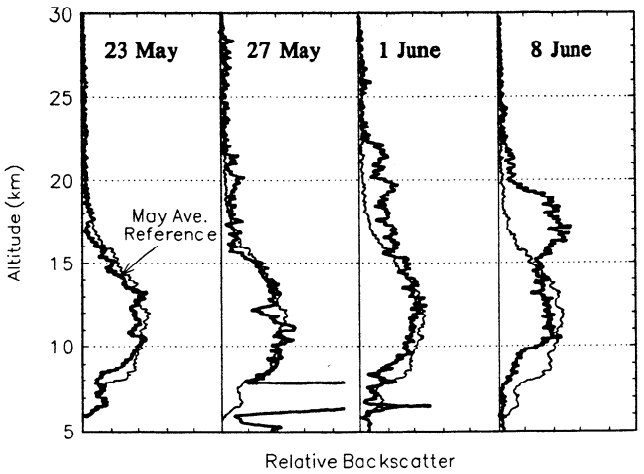

Figure 4. University of Rome lidar backscatter profiles taken over the South Pole on the dates indicated.

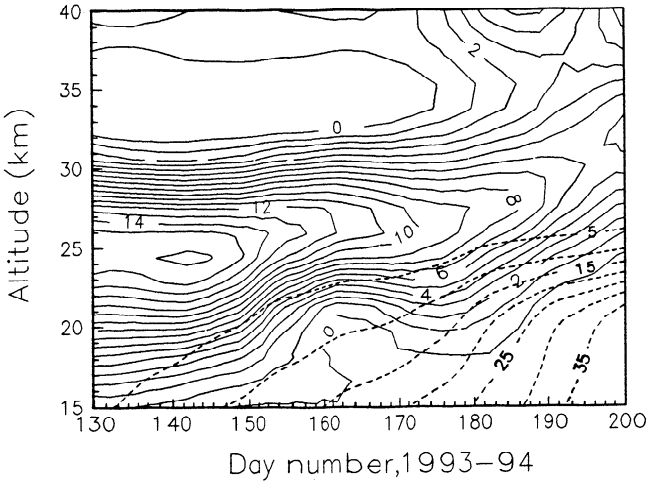

Figure 5b. Retrieved HNO_3 profile contours as in Figure 5a, overlaid with contours showing integrated volume of STS following the formulation of *Carslaw et al.* [1995]. Temperature and HNO_3 profiles as a function of time were taken from Figure 5a. H_2O and H_2SO_4 were set at constant mixing ratios of 5 ppmv and 0.5 ppbv, respectively. STS is given in $\mu m^3/cm^3$.

evolution of HNO_3 loss versus altitude, temperature, and time is complicated by vertical transport during this period [*Crewell et al.*, 1995; *Manney et al.*, 1994; *Rosenfield et al.*, 1994]. For instance, air at 30 km, with an HNO_3 mixing ratio of ~4 ppbv on day 130, will have moved down to about 28 km by day 180, replacing air that was carrying ~11 ppbv at that altitude on day 130. Descent rates increase with altitude, being about 20 m/d for air starting at ~20 km, 40 m/d for air starting at ~30 km [*Crewell et al.*, 1995], and up to 250 m/d for air starting at ~50 km. It is significant that this descent is not apparent in the HNO_3 contours, which if anything show a small increase in mixing ratio at constant altitude in the 28-32 km range up to about day 175. This may indicate a continued conversion of NO_x into HNO_3 as air descends from higher altitudes. It is nevertheless clear that in the region below 30 km, HNO_3 depletion tracks the upward progression of temperatures $\leq$196 K, at least up to about day 180. (We discuss the middle stratospheric behavior following day 180 in the next section along with the separate phenomenon of the sudden appearance of HNO_3 in the upper stratosphere starting after day 170).

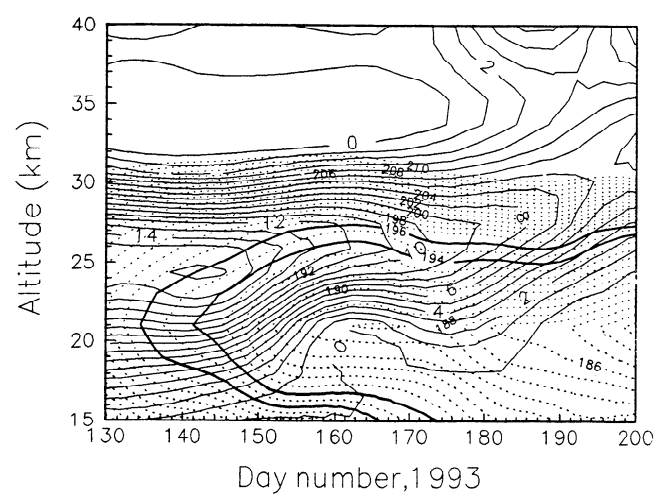

Figure 5a. Enlargement of the altitude region and time period of HNO_3 condensation from Figure 1. Solid thin contour and large numbers give HNO_3 in ppbv. The dotted contours and smaller numbers give values for local measurements of temperature in K. The heavy solid lines mark temperature contours at 194 and 196 K.

The May average background lidar backscatter depicted in Figure 4 is that from the persistent lower stratospheric sulfate aerosol layer, supplemented by aerosols remaining from Mount Pinatubo. The rapid increment in backscatter above 15 km seen in Figure 4 is the result of PSC formation. Nitric acid dihydrate (NAD), nitric acid trihydrate (NAT) and possibly higher hydrates, plus supercooled ternary solutions (STS) composed of HNO_3 accreted on H_2SO_4-H_2O aerosols, have all been proposed for PSCs; all have a formation temperature several degrees higher than the frost point of pure water for typical stratospheric conditions. Each has a somewhat different range of formation temperatures, depending on partial pressures of constituent species, which in turn varies with altitude [e.g., *Marti and Mauersberger*, 1993, 1994; *Beyer et al.*, 1994; *Song*, 1994; *Carslaw et al.*, 1994, 1995, and references therein].

In Figure 5b we have applied the formulation for STS accretion given by *Carslaw et al.* [1995] as a function of temperature, pressure, and constituent abundance, along with the local temperature field and day-by-day HNO_3 profiles from our own data, to compute the integrated day-by-day STS volume in $\mu m^3/cm^3$. The trend of computed STS volume increase tracks the depletion

of HNO_3 rather well as a function of time and altitude. A plot of the frost point for NAT formation as a function of altitude and temperature [*Hanson and Mauersberger*, 1988] (not shown) appears to give a poorer fit to the HNO_3 depletion contours. We also note that the appearance of the first lidar-detected PSCs on about day 148, and the altitude range of growth over the next several days (Figure 4), both agree rather well with the STS accretion curves of Figure 5b. Nevertheless, given the experimental uncertainties involved and the small range within which the temperature and other variables determine one accretion mechanism or another, it seems likely that only high-resolution in situ measurements will be able to fully determine the details of PSC formation and composition.

3.2 Midwinter

Formation of new high-altitude HNO_3. Figure 6 shows a series of spectra from the period June 21 to July 22 (days 172 to 203). These spectra are strikingly different from those seen earlier. Individually resolved emission lines are almost always present during this period, when none could be seen previously, indicating significant new emission from the middle to upper stratosphere. We stress that the optical density of the entire HNO_3 column is always very small, so that self-absorption by lower stratospheric HNO_3 cannot block out the emission from higher layers whenever the latter is present. Figure 7 shows a sample of retrieved profiles, and the overall evolution of the high-altitude mixing ratios can be seen in Figure 1. The generation of significant high-altitude HNO_3 appears to be a relatively brief

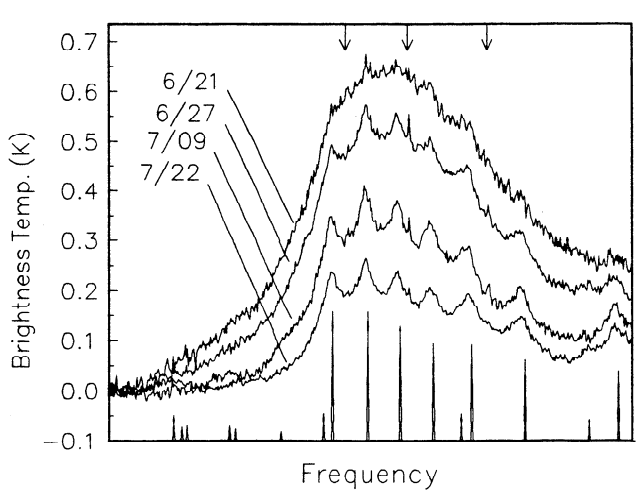

Figure 6. Sample spectra for the period June 21 to July 22, 1993, indicating the rapid growth of emission from high-altitude nitric acid vapor. The arrows at the top indicate the positions of 3 weak, narrow mesospheric emission lines of NO_2 which make their first appearance before the middle of May. Individual HNO_3 line positions and relative strengths are indicated along the bottom, as in Figure 2.

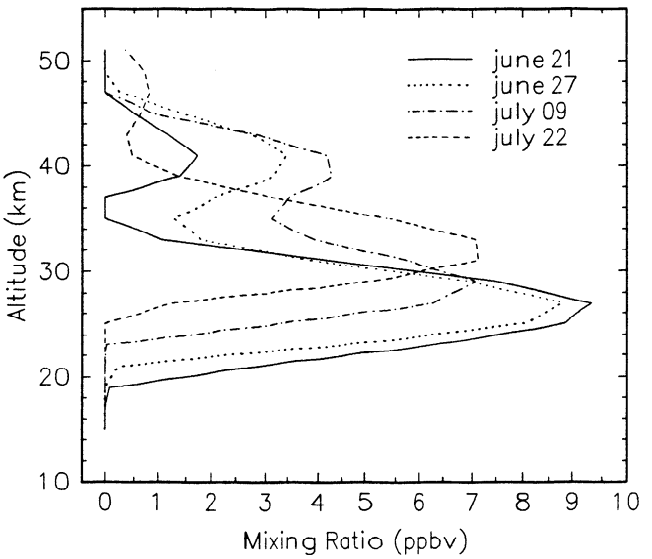

Figure 7. Mixing ratio profiles retrieved from the spectra shown in Figure 6. See text for commentary about the profile for July 22.

phenomenon with a rapid onset in the 1993 data, followed by downward transport common to all vortex air during winter, as discussed in the previous section, until we can no longer resolve the profile into separate layers. Retrievals are, however, consistent with the continued, perhaps intermittent, generation of small amounts of HNO_3 near or above 40 km up to mid-August.

A large increase of gas-phase HNO_3 in the polar winter middle stratosphere was first observed by the short-lived LIMS instrument during the northern winter of 1978-1979 [*World Meteorological Organization/NASA (WMO/NASA)*, 1986, and references therein], but remained essentially unexplained, despite various efforts to identify a transport or in situ generation mechanism [e.g., *Austin et al.*, 1986; *Jackman et al.*, 1987]. In the LIMS data, HNO_3 enhancement in the winter stratosphere appears as a relatively smooth gradient tapering off above the lower stratospheric distribution [e.g., *WMO/NASA*, 1986, p. 559]. No further observations were available to confirm the LIMS data until a set of observations by the CLAES instrument on UARS, and the set presented here. CLAES observations were made near both poles during its active lifetime from October 1991 to June 1993, and data for the Arctic winter of 1991-1992 have recently been analyzed by *Kawa et al.* [1995]. In that data, development of a distinct upper layer of HNO_3 was seen in the winter middle stratosphere, peaking around 4 mbar (~34 km) in the CLAES retrievals.

Garcia and Solomon [1994] recently proposed that an extension of the observed distribution of stratospheric "aerosol" beyond the upper limit of observational detection (~32 km) could furnish a mechanism for nitric acid production. They assumed an exponential decrease with a scale height of 7 km and concluded that the re-

sulting surface area is large enough for heterogeneous reaction of N_2O_5 with H_2O to generate a relatively large amount of HNO_3, if a surface reaction probability of 0.1 is assumed. Although qualitatively reasonable, there may be problems with this explanation. (1) Recent laboratory work by *Zhang et al.* [1995] suggests that the surface reaction probability on H_2SO_4-H_2O aerosols can be significantly lower than 0.1 in the presence of HNO_3. (2) The observed vertical distribution of new HNO_3 in late June to early July does not taper off smoothly from lower altitudes, as the assumed aerosol content drops, but lies in a reasonably well-defined second layer. (3) The presumed first step in HNO_3 generation involves the nighttime conversion of NO_2 and NO_3 into N_2O_5. This reaction occurs relatively rapidly (on the order of a few days) at night even as high as 40 km [e.g., *Brasseur and Solomon,* 1984, p. 262], and subsequent heterogeneous reaction of $N_2O_5 + H_2O \rightarrow 2\ (HNO_3)$ will be very rapid, yet the high-altitude layer does not appear until middle to late June. The Garcia and Solomon scenario does not appear to explain this delay. (4) Particularly rapid downward transport begins in the middle to upper stratosphere significantly before sunset [*Rosenfield et al.,* 1994; *Cheng et al.,* 1996] and continues at lesser rates at all altitudes throughout the winter. The aerosol profile postulated by Garcia and Solomon should thus be diminished well before the time of HNO_3 formation.

The first appearance of emission significantly above noise level at ~40 km occurred in our data about June 21 (with weak hints a few days prior), i.e., about a month after the entire region poleward of 75° has entered winter darkness at 40-km altitude. Table 1 gives the dates of sunset and sunrise at both 75° and 80°S, and the dates before or after which there is at least 5 hours of daylight per day. Delays of about a month have been noted in the early LIMS data [*Austin et al.,* 1986] and in the CLAES data as well [*Kawa et al.,* 1995]. We thus believe the delay observed between sunset and the appearance of high-altitude HNO_3 in our own observations is not primarily due to an accident of vortex positioning or transport over our particular observing site.

Kawa et al. [1995] have reviewed an ion cluster mechanism first investigated by *Bohringer et al.* [1983], and point out several attractive features which make it plausible as a mechanism for providing sufficient surface area for heterogeneous N_2O_5 conversion in the ~40 km range, but confirmation of this mechanism will require further measurements.

In concluding this discussion, we note in passing the appearance of weak, very narrow emission lines of NO_2 in the spectral bandpass for HNO_3 (see particularly Figure 6), which strengthen around the time of appearance of new HNO_3 in the 40-km range. The narrowness of the former places them at least 10-15 km above the region of HNO_3 formation, but continuous downward transport from early winter may furnish some of the source of supply for new HNO_3.

The midwinter middle stratosphere. We address next a peculiar feature seen in the contour plots of Figures 1 and 5: by about day 190, HNO_3 appears to diminish rapidly in the 26 to 30-km range, while temperatures remain essentially constant and are significantly above the condensation threshold. We believe that this can be attributed to the effects of downward transport (see previous section) finally winning out over the heterogeneous conversion of residual NO_x to gas-phase HNO_3. Shortly afterward, by day 200, HNO_3 appears to increase rapidly in the 30 to 35-km region (a sample of the corresponding profile evolution is shown in Figure 7: note the profile shown for July 22). We believe the latter is likely to be an artifact of the profile retrieval process, caused by decreasing separation of the upper and lower HNO_3 layers over time due to the quite different rates of descent as a function of altitude [*Manney et al.,* 1994; *Rosenfield et al.,* 1994; *Crewell et al.,* 1995]. Starting at 40 km around day 180, the upper layer would have moved several kilometers closer to the lower layer by about day 210 (see previous section for approximate values of downward transport rate versus altitude), assuming a brief period of generation and a relatively long lifetime. Tests on the multiple line spectrum of HNO_3 show that two layers may be difficult to resolve, depending somewhat on relative mixing ratio

Table 1. Sunset and Sunrise as a Function of Latitude and Altitude

Latitude	Z,km	≥5 Hours Sun	Sunset	Sunrise	≥5 Hours Sun
-75	30	May 11	May 23	July 21	Aug. 3
		(131)	(143)	(202)	(215)
	45	May 16	June 1	July 14	July 29
		(136)	(151)	(195)	(210)
-80	30	April 27	May 3	Aug. 11	Aug. 17
		(117)	(123)	(223)	(229)
	45	May 1	May 8	Aug. 6	Aug. 13
		(121)	(128)	(218)	(225)

Numbers in parentheses are day numbers for given dates.

and thickness, when their centers are closer than ~8-10 km, and may appear as a single thick layer centered at the mean altitude (see appendix). This is quite like the transition in profile shape with time seen in Figure 7. We therefore caution against the unqualified acceptance of the profiles or contours retrieved during the period from about day 200 to at least 225. We believe it likely that the upper layer descends in approximate accordance with the rates given by *Rosenfield et al.* [1994] as a function of altitude and time, while what remains of the lower layer also descends at a correspondingly smaller speed.

The individually resolved emission lines of HNO_3 rather abruptly fade away between August 10, when they were still clearly visible, and August 13 when they dropped to barely above the detection limit. This middle stratospheric emission did not return again in any significant strength above noise level for the remainder of the season. This timing qualitatively agrees with the first appearance of sunlight at latitudes close to the pole (see Table 1), and the rather short lifetime (on the order of 1 day) against photolysis for HNO_3 in the daylit middle stratosphere [e.g., *Austin et al.*, 1986].

3.3. The Spring-Summer Recovery Period

The most notable feature of the spring-summer period is the very slow increase of HNO_3 in the lower stratosphere (Figures 1 and 8). If release of HNO_3 occurred when PSCs in the 15 to 25 km range evaporate (whether composed of NAD, NAT, or STSs), an increase in emission intensity would be immediate. An excess of HNO_3 (formed via denitrifying heterogeneous reactions during winter) would then remain for several weeks until photolysis restored equilibrium between HNO_3 and other NO_x. We conclude that when HNO_3 was released from the particles on which it initially accreted, it was pressure-broadened beyond our ability to detect it, indicating that these particles had gravitationally settled several kilometers. It is interesting to note that well over a decade ago, the presence of an "aerosol hole" over Antarctica in October was taken to indicate the net removal of particles by sedimentation during the winter [e.g., *Hamill and McMaster*, 1984]. It seems clear that re-nitrification of the Antarctic lower stratosphere does not come primarily from the photolysis of HNO_3 released by PSC evaporation.

The 1992 total column measurements of *Van Allen et al.* [1995] from an infrared spectrometer are qualitatively very similar to our 1993-1994 measurements, when our retrieved profiles are integrated to give column densities, as in Figure 8. Quantitatively, our column densities are smaller by an offset of $\sim 0.5 \times 10^{16}$ molecules/cm^2 throughout the year, but we present here only values integrated above 15 km, whereas the column measurements of Van Allen et al. run from the ground up. The offset quoted above is not unreasonable for the column correction below 15 km. An additional source

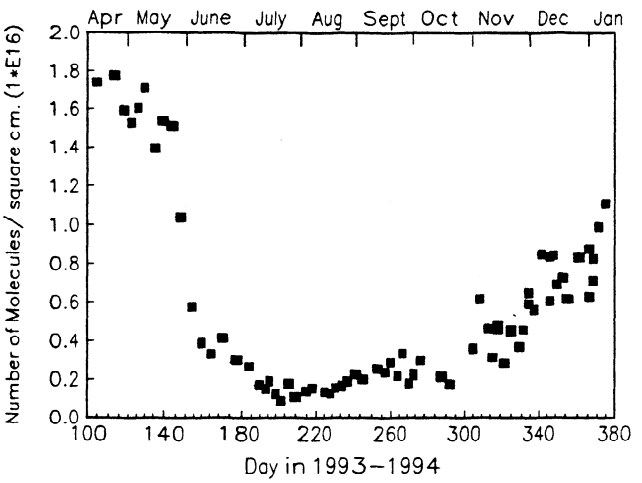

Figure 8. Column densities derived by integration of retrieved profiles from 15 km upward. Accuracy is believed to be $\pm 0.1 \times 10^{16}$ molecules/cm^2 or better.

of systematic error might arise from the assumed vibrational line strength used in reducing the infrared spectroscopic observations of Van Allen et al.: the quoted accuracy here is 10%. A more interesting and significant difference in the two data sets is that the onset of rapid HNO_3 depletion occurred more than a full month earlier in 1993 than in 1992. It is confirmed by additional unpublished 1993 South Pole column density measurements by the University of Denver (F. Murcray, private communication, 1995).

Finally, we note a significant lack of closure in the recovery of HNO_3 by the time of our last measurement on January 10, 1994, and the values measured at the start of our observations in mid-April of 1993. Assuming similar column densities were reached by mid-April 1994, then essentially half the total increase in HNO_3 above 15 km would appear in the Antarctic stratosphere during the 3-month interval between mid-January and mid-April, well after the breakdown of the vortex. Southern hemisphere retrievals of HNO_3 at a single altitude of $\theta = 465$ K (~19 km) have been published for selected periods between late April and early November 1992, from UARS CLAES data by *Roche et al.* [1994] and from UARS MLS data by *Santee et al.* [1995]. Both studies show that in mid-August a ring of enhanced HNO_3 encircled Antarctica at latitudes <75°S with mixing ratios up to 10-13 ppbv. By November 1, this ring had largely dissipated at θ =465 K, and although mixing ratios near the pole recovered from the extreme lows of August, it does not appear that this was accomplished by a significant poleward transfer of the large ring mixing ratios, at least not at the constant pressure altitude used in the MLS analysis. The data set of Van Allen et al. begins in late January 1992 and shows an increase of about 25% up to the time of rapid depletion, for the estimated column density above 15 km, but clearly not a doubling, suggesting some interannual differences in

depletion and recovery. *Roche et al.* [1994] in their Figure 5b show a much earlier and more complete recovery for the 1992-1993 spring-summer period (one also marked by the heaviest Pinatubo-driven aerosol concentrations), but this is for a zonal average from 72° to 80°S at a fixed altitude of 46 mbar (≃460 K or 19 km).

What is the ultimate fate of HNO_3 removed from the stratosphere? It is interesting to note that the total column measurements of Van Allen et al. from the surface up show no rebound in gas-phase HNO_3 after a time sufficient for PSC settling to low altitudes and higher temperatures. This may indicate removal from the vortex region by transport in the outflow of air to lower latitudes which must occur above the tropopause. On the other hand, if gravitational settling causes penetration of the tropopause while still within the vortex region, then increasing water vapor below the tropopause might allow a rapid accretion of water onto STS surfaces, which would both trap the HNO_3 and greatly increase the rate of gravitational settling. It is not implausible to assume particles might move from the stratosphere to the surface in a matter of months. *Qin et al.* [1992] give figures for total nitrogen deposition in surface snow at a series of locations across Antarctica (unfortunately labeled nitrate in their Figures 2 and 3; see *Moore,* [1993] and *Qin et al.* [1993] for clarifications). Concentrations are greatest at high interior regions, but Qin et al. conversely give lower fluxes for these regions, dividing observed concentration by total estimated snowfall, which is greatest for coastal regions. Taking the column change in stratospheric gas-phase HNO_3 between the early winter maximum and the early summer recovery period to be $\sim 1.6 \times 10^{16}$ molecules/cm^2, and assuming all this reaches the surface in one year, the annual flux would be about 1.6×10^{26} molecules of HNO_3/km^2, or about 3.7 kg/km^2, surprisingly close to the figure given by Qin et al. for total nitrogen flux near the pole from all sources (1.5-4 kg/km^2/yr, which they assume to be derived primarily from atmospheric, but not necessarily stratospheric, sources) and more than a factor of 2 below the highest fluxes listed at other high inland sites between the pole and Vostok Station. Snowfall is notoriously difficult to measure in Antarctica, however, so that the derived fluxes could be in error by a significant factor (see *Moore* [1993], for instance). Moreover, Qin et al. take no account of the role of katabatic winds in scouring the high mid-continent and sweeping material toward or beyond coastal areas throughout the winter. It is at least interesting that the result of the simple assumptions used here is of the same order of magnitude as the estimated total nitrogen flux. Clearly, more observations are needed to clarify the fate of HNO_3 lost in the winter.

4. Summary

In the present study, measurements of pressure-broadened spectral lines were taken every few days from April 15, 1993 to January 10, 1994. From these, vertical profiles and column densities have been retrieved for the altitude range from ~15 to 48 km. We have been able to directly link the initial appearance of PSCs detected from local lidar observations with the onset of rapid removal of HNO_3 from the lower stratosphere, to show the shifting altitude range of initial and subsequent removal as a function of evolving temperatures, to determine the total amount of depletion above ~15 km, and to document the slow increase of HNO_3 in the 1993-1994 Antarctic lower stratosphere through the spring, summer, and early fall period. We note that the depletion of gas-phase HNO_3 by condensation occurred a month earlier in 1993 than seen by *Van Allen et al.* [1995] in their 1992 column measurements. We show that the rate of loss of gas-phase HNO_3 over a vertical range of several kilometers is consistent with theoretical expectations of temperatures and partial pressures for the formation of ternary PSCs composed of HNO_3, H_2O, and H_2SO_4. The very slow recovery of gas-phase HNO_3 after atmospheric warming is strong proof that gravitational settling carries condensed particles significantly below ~15 km by the end of winter: the slow recovery in ground-based total column measurements by Van Allen et al. further indicates that this material does not remain in the lower atmosphere over the polar region until warming occurs. We speculate on the fate of HNO_3 removed from the gas phase by condensation during the polar winter.

We have also observed the formation of new HNO_3 in the middle to upper stratosphere during late June and early July, as initially seen in 1978-1979 LIMS data from the northern polar stratosphere, and more recently in CLAES data [*Kawa et al.,* 1995]. By later July and August, our measurements indicate that the initial, separate high layer was transported downward, as part of the general differential vertical transport in the polar vortex, until it became too close to the remnants of the "normal" lower layer to be resolved by our retrieval technique. There is also evidence for continued or intermittent formation of smaller amounts of HNO_3 at or above ~40 km up to mid-August.

Appendix

We use an iterative constrained matrix inversion technique [*Twomey,* 1977; *Puliafito et al.,* 1995] to retrieve nitric acid mixing ratio profiles from pressure-broadened emission lines. This technique can handle the inversion of several lines simultaneously and is thus well suited to the cluster of HNO_3 lines in our spectra. We illustrate retrieval accuracy by starting with assumed "true" profiles similar to various stratospheric distributions of HNO_3. From these, we generate synthetic spectra, add an appropriate level of random noise, and test the degree to which profiles retrieved from the artificial data match the initial profiles.

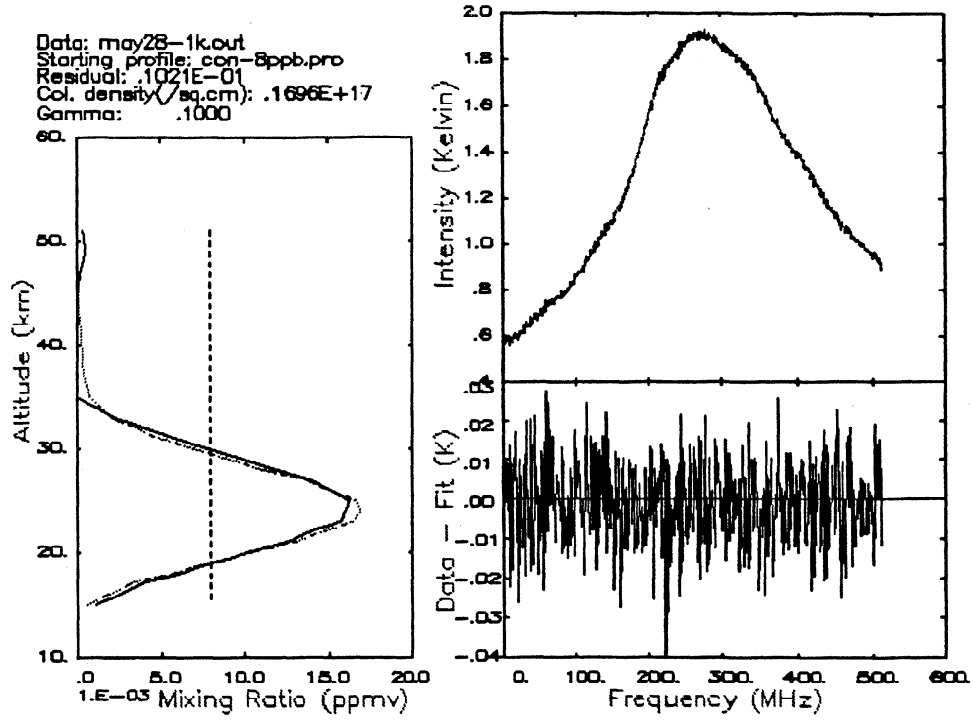

Figure A1. Profile retrieval test using iterative constrained matrix inversion. (Left) Dotted line is "true" profile, dashed line is initial guess, and solid line is retrieved profile. (Upper right) Spectrum synthesized from "true" profile, with 0.01 K rms random noise added. Superimposed is the fit generated from the retrieved profile, lying everywhere within the noise. (Lower right) The (data − fit) residuals for all 512 spectral channels, which have a resolution of 1 MHz each.

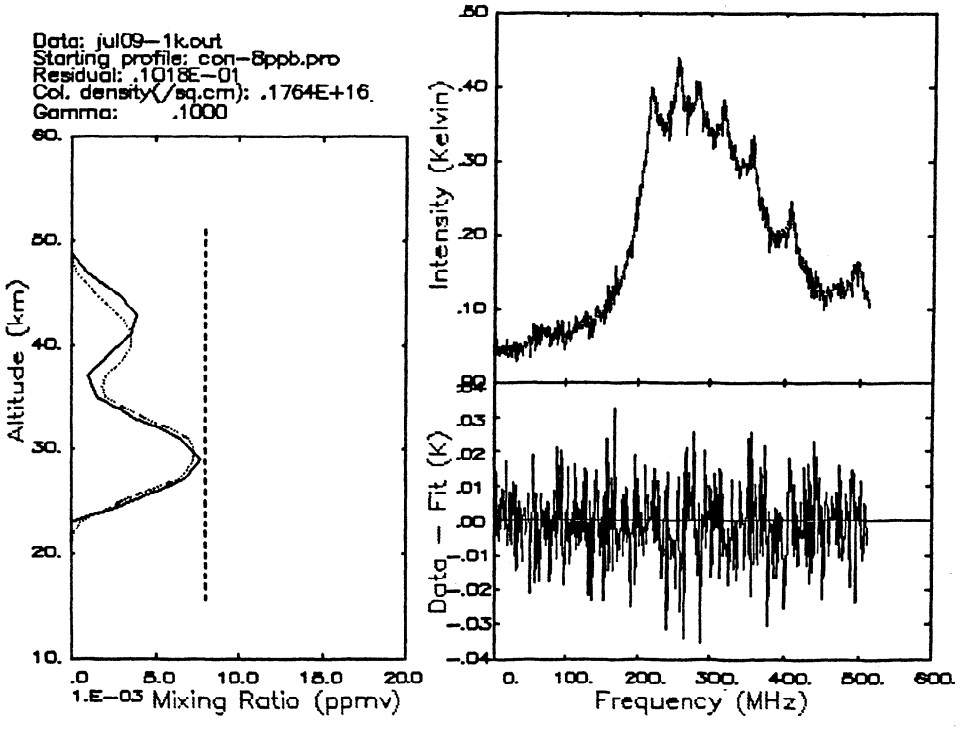

Figure A2. Profile retrieval as in Figure A1, but assuming a lower layer strongly depleted below 30 km and an upper layer peaking at about 41 km, as found around day 190. Again 0.01 K rms random noise has been added to the synthesized spectrum before deconvolution. Despite the significantly worse S/N ratio, retrieval accuracy is still quite good, except for a upward shift of ~1.5 km in the upper layer.

Tests were made using spectral contributions synthesized from significant nitric acid lines centered outside as well as inside the spectral passband of our instrument. This so-called forward synthesis is unambiguous and unique in spectral output. It is well known that all methods of retrieval by deconvolution from even noise-free data are in principle non-unique [e.g., *Twomey*, 1977]: the addition of noise further adds to the retrieval uncertainty in nonlinear proportion to the signal/noise ratio. For the tests made here, random channel-to-channel noise at an rms value of 0.01 K in brightness temperature was then added to the synthetic spectra. This amplitude is typical or somewhat larger than the sum of random receiver plus sky noise emission in our spectra. Figure A1 gives an illustration of a representative vertical profile recovery using the iterative constrained matrix inversion technique. The left-hand panel shows the "true" profile (dotted line) used to generate the spectrum. This was similar to those found in the April-May period. The upper right panel shows the generated spectrum, with noise added, which acts as "data" for retrieval testing. The solid curve in the left-hand panel is the retrieved profile, and superimposed on the "data", but rather difficult to see in this case, is the noise-free synthetic spectrum generated from the retrieved profile. The difference spectrum is shown in the lower right panel. Finally, the starting profile used for the iterative constrained inversion is shown as the dashed line in the left-hand panel. We have found that results from this method of deconvolution are essentially immune to the choice of any "reasonable" profile (i.e., within an order of magnitude at any given altitude) used to start the iterative solution. We illustrate here the use of a constant 8 ppbv mixing ratio from 15 to 51 km as the starting profile. Note in particular the ability of the technique to find very nearly the correct mixing ratio at the highly pressure-broadened low end of the distribution.

All examples here were processed with an identical fourth-order derivative constraint. No attempt was made to simulate small instrumental artifacts contributed by standing wave reflections in the input path of the instrument, or from other sources. Unless these are of rather wide extent (e.g., producing an undulation with a "wavelength" one or two times the spectral spread of 512 MHz), or of large amplitude (several tens of milli-Kelvin), we have found that such artifacts tend to have a rather small effect on retrieval accuracy. In actuality, our data (e.g., Figures 2 and 6) show only minor standing wave artifacts, with a few exceptions which have been discarded if retrievals differed significantly from near-temporal neighbors.

Figure A2 shows retrieval of a lower layer similar to that in Figure A1, but strongly depleted below 30 km, and with an assumed upper layer formed with a peak at 41 km. Retrieval of both the lower layer peak altitude and shape is quite good, while the upper layer is somewhat displaced in the retrieval. Figure A3 indicates

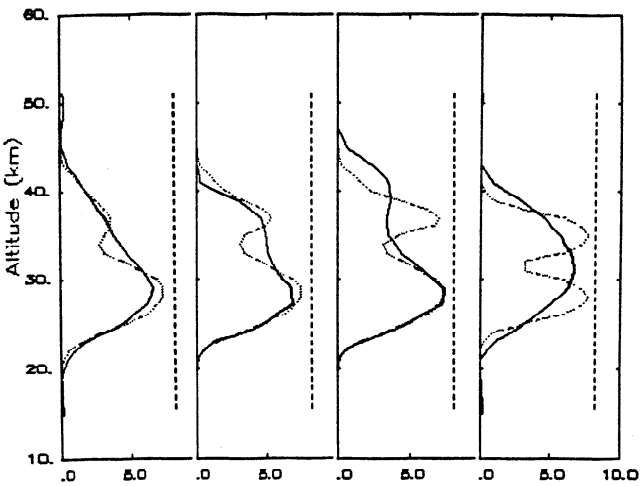

Figure A3. Profile retrieval as in Figure A2, but with the layers moved downward to a peak separation of ~8 km. Retrievals from "forward" line shape syntheses for each of four profiles (dotted lines) are tested, with increasing mixing ratios in the upper layer, as well as a thicker upper layer in the last. Residual fits are about as shown in Figures A1 and A2 for each case tested.

potential problems with retrieval of a double-layer profile when the lower layer in Figure A2 has been moved down by 1 km and the upper layer by 4 km. The fit to the "data" and resulting residuals were essentially as shown in Figures A1 and A2, and so are not repeated. Now, depending on the assumed amplitude and thickness of the upper layer, various results follow, varying from fairly good for a weak layer to total blending into one layer peaking at the mean altitude for two thick layers of equal mixing ratio. Since differential vertical transport will bring upper and lower layers together during the course of a winter, we caution against more than a provisional acceptance of the midwinter profiles retrieved here (from about days 200-250).

Aside from questions of midwinter retrieval accuracy, recovery of the peak mixing ratios for upper or lower layers appears to be accurate to a few percent in these illustrations. We estimate a more conservative 10-15% uncertainty for profiles retrieved from actual data. There are additional uncertainties connected with receiver sensitivity calibration, intrinsic emission line strength accuracy, pressure and temperature profiles from local balloon and satellite measurements, and atmospheric opacity corrections: we estimate these to sum in quadrature to an additional 15% for our HNO_3 data. The latter constitute a systematic uncertainty for any given day's data, but the total is composed of individual contributions, the largest of which vary in a random manner from one day to another. We therefore add the deconvolution uncertainty to the parameter uncertainties in quadrature for an overall uncertainty estimate of 21%.

Acknowledgments. This work was supported by grant OPP-9117813 from the National Science Foundation, with additional support from NASA grants NAGW-2182 and NAGW 1-1354. We thank Giorgio Fiocco for making available the University of Rome LIDAR backscatter data prior to publication, Susan Solomon for pointing out the 1979 LIMS data at an early stage, and Randy Kawa for making available a prepublication copy of his manuscript detailing CLAES observations of HNO_3 as well as additional unpublished observations. D. Cheng supplied ozone background spectra used in data analysis.

References

Austin, J., R. R. Garcia, J. M. Russell III, S. Solomon, and A. Tuck, On the atmospheric photochemistry of nitric acid, *J. Geophys. Res., 91,* 5477-5485, 1986.

Beyer, K. D., S. W. Seago, H. Y. Chang, and M. J. Molina, Composition and freezing of aqueous H_2SO_4/HNO_3 solutions under polar stratospheric conditions, *Geophys. Res. Lett., 21,* 871-874, 1994.

Bohringer, H., D. W. Fahey, F. C. Fehsenfeld, and E. E. Ferguson, The role of ion-molecular reactions in the conversion of N_2O_5 to HNO_3 in the stratosphere, *Planet. Space Sci., 31,* 185-191, 1983.

Brasseur, G. and S. Solomon, *Aeronomy of the Middle Atmosphere*, 1st ed., D. Reidel, Norwell, Mass., 1984.

Carslaw, K. S., B. P. Luo, S. L. Clegg, T. Peter, P. Brimblecombe, and P. J. Crutzen, Stratospheric aerosol growth and HNO_3 gas phase depletion from coupled HNO_3 and water uptake by liquid particles, *Geophys. Res. Lett., 21,* 2479-2482, 1994.

Carslaw, K. S., B. Luo, and T. Peter, An analytic expression for the composition of aqueous HNO_3-H_2SO_4 stratospheric aerosol including gas phase removal of HNO_3, *Geophys. Res. Lett., 22,* 1877-1880, 1995.

Cheng, D., R. L. de Zafra, and C. Trimble, Millimeter-wave spectroscopic measurements over the South Pole, 2, An 11-month cycle of stratospheric ozone observations during 1993-94, *J. Geophys. Res.,* in press, 1996.

Coffey, M. T., W. G. Mankin, and A. Goldman, Airborne measurements of stratospheric constituents over Antarctica in the austral spring 1987, 2, Halogen and nitrogen trace gases, *J. Geophys. Res., 94,* 16,597-16,613, 1989.

Crewell, S., D. Cheng, R. L. de Zafra, and C. Trimble, Millimeter-wave spectroscopic measurements over the South Pole, 1. A study of stratospheric dynamics using N_2O observations, *J. Geophys Res., 100,* 20,839-20,844, 1995.

Crownover, R. L., R. A. Booker, F. C. De Lucia, and P. Helminger, The rotational spectrum of nitric acid: The first five vibrational states, *J. Quant. Spectrosc. Radiat. Trans., 40,* 39-46, 1988.

Garcia, R., and S. Solomon, A new numerical model of the middle atmosphere 2. Ozone and related species, *J. Geophys. Res., 99,* 12,937-12,951, 1994.

Goyette, T. M., W. L. Ebenstein, Frank De Lucia, and P. Helminger, Pressure broadening of the millimeter and submillimeter wave spectra of nitric acid by oxygen and nitrogen, *J. Molec. Spectrosc., 128,* 108-116, 1988.

Hamill, P., and L. R. McMaster, Polar stratospheric clouds: Their role in stratospheric processes, *NASA Conf. Publication CP-2318,* 1984.

Hanson, D., and K. Mauersberger, Laboratory studies of the nitric acid trihydrate: Implications for the south polar stratosphere, *Geophys. Res. Lett., 15,* 855-858, 1988.

Jackman, C. H., P. D. Guthrie, and J. A. Kaye, An intercomparison of nitrogen-containing species in Nimbus 7 LIMS and SAMS data, *J. Geophys. Res., 92,* 995-1008, 1987.

Kawa, S. R., J. B. Kumer, A. R. Douglass, A. E. Roche, S. E. Smith, F. W. Taylor, and D. J. Allen, Missing chemistry of reactive nitrogen in the upper stratospheric polar winter, *Geophys. Res. Lett., 22,* 2629-2632, 1995.

Manney, G. L., R. W. Zurek, A. O'Neill, and R. Swinbank, On the motion of air through the stratospheric polar vortex, *J. Atmos. Sci., 51,* 2973-2994, 1994.

Marti, J. J., and K. M. Mauersberger, Laboratory simulations of PSC particle formation, *Geophys. Res. Lett., 20,* 359-362, 1993.

Marti, J. J., and K. M. Mauersberger, Evidence for nitric acid pentahydrate formed under stratospheric conditions, *J. Phys. Chem., 98,* 6897-6899, 1994.

Moore, J. C., Comment on "The distribution of nitrate content in the surface snow of the antarctic ice sheet along the route of the 1990 International Trans-Antarctic Expedition" by Quin Dahe, Edward J. Zeller, and Gisela A. M. Dreschhoff, *J. Geophys. Res., 98,* 6181-6183, 1993.

Murcray, F. J., F. H. Murcray, A. Goldman, D. G. Murcray, and C. P. Rinsland, Infrared measurements of several nitrogen species above the South Pole in December 1980 and November-December 1986, *J. Geophys. Res., 92,* 13,373-13,376, 1987.

Murcray, F. J., A. Goldman, A. Matthews, R. D. Blatherwick, and N. B. Jones, HNO_3 and HCl amounts over McMurdo during the spring of 1987, *J. Geophys. Res., 94,* 16,615-16,618, 1989.

Puliafito, E., R. Bevilacqua, J. Olivero, and W. Degenhardt, Retrieval error comparison for several inversion techniques used in limb-scanning millimeter-wave spectroscopy, *J. Geophys. Res., 100,* 14,257-14,268, 1995.

Qin, D., E. J. Zeller, and G. A. M. Dreschhoff, The deposition of nitrate content in the surface snow of the antarctic ice sheet along the route of the 1990 International Trans-Antarctic Expedition, *J. Geophys. Res., 97,* 6277-6284, 1992.

Qin, D., E. J. Zeller, and G. A. M. Dreschhoff, Reply, *J. Geophys. Res., 98,* 6185-6186, 1993.

Roche, A. E., J. B. Kumer, and J. L. Mergenthaler, CLAES observations of $ClONO_2$ and HNO_3 in the Antarctic stratosphere, between June 15 and September 17, 1992, *Geophys. Res. Lett., 20,* 1223-1226, 1993.

Roche, A. E., J.B. Kumer, J. L. Merganthaler, R. W. Nightingale, W. P. Uplinger, G. A. Ely, J. F. Potter, D. J. Wuebbles, P. S. Connell, and D. E. Kinnison, Observations of lower-stratospheric $ClONO_2$, $HNO_3$and April 1993, *J. Atmos. Sci., 51,* 2877-2902, 1994.

Rosenfield, J. E., P. A. Newman, and M. R. Schoeberl, Computations of diabatic descent in the stratospheric polar vortex, *J. Geophys. Res., 99,* 16,677-16,689, 1994.

Santee, M. L., W. G. Read, J. W. Waters, L. Froidevaux, G. L. Manney, D. A. Fowler, R. F. Jarnot, R. S. Harwood, and G. E. Peckham, Interhemispheric differences in polar

stratospheric HNO_3, H_2O, ClO, and O_3 from UARS MLS, *Science, 267*, 849-852, 1995.

Song, N., Freezing temperatures of $H_2SO_4/HNO_3/H_2O$ mixtures: Implications for polar stratospheric clouds, *Geophys. Res. Lett., 21*, 2709-2712, 1994.

Toon, G. C., C. B. Farmer, L. L. Lowes, P. W. Schaper, J-F. Blavier, and R. H. Norton, Infrared aircraft measurements of stratospheric composition over Antarctica during September, 1987, *J. Geophys. Res., 94*, 16,571-16,596, 1989.

Twomey, S., Introduction to the mathematics of inversion in remote sensing and indirect measurements, in *Developments in Geomathematics*, vol. 3, Elsevier Sci., New York, 1977.

Van Allen, R., X. Liu, and F. J. Murcray, Seasonal variation of atmospheric nitric acid over the South Pole in 1992, *Geophys. Res. Lett., 22*, 49-52, 1995.

Williams, W. J., J. J. Kosters, and D. G. Murcray, Nitric acid densities over Antarctica, *J. Geophys. Res., 87*, 8976-8980, 1982.

WMO/NASA, Atmospheric Ozone 1985: Assessment of our understanding of processes controlling its present distribution and change, *Rep. 16*, 3 vols., Global Ozone Res. and Monit. Proj., Geneva, 1986.

Zhang, R., M. Leu, and L. F. Keyser, Hydrolysis of N_2O_5 and $ClONO_2$ on the $H_2SO_4/HNO_3/H_2O$ ternary solutions under stratospheric conditions, *Geophys. Res. Lett., 22*, 1493-1496, 1995.

R. L. de Zafra and S. Crewell, Department of Physics, State University of New York, Stony Brook, NY 11794. (e-mail: rdezafra@ccmail.sunysb.edu)

V. Chan, Department of Mathematics, Iowa State University, Ames, IO 50011.

J. M. Reeves, AOSS Department, University of Michigan, Ann Arbor, MI 48109.

C. Trimble, 4908 1st Parkway, Sacramento, CA 95823

(Received August 22, 1995; revised November 27, 1995; accepted November 27, 1995.)